*SF2A 2021*
*A. Siebert, K. Baillié, E. Lagadec, N. Lagarde, J. Malzac, J.-B. Marquette, M. N'Diaye, J. Richard, O. Venot (eds)*

# SPECTRAL EVOLUTION OF ALFVÉNIC TURBULENCE

R. Grappin[1], A. Verdini[2] and W.-C. Müller[3]

**Abstract.** A correct description of solar wind acceleration relies critically on a good understanding of the turbulent cascade in the solar wind. However, no cascade theory is presently able to reproduce the variability of the observed spectral indices in the large scale range of the spectrum (Grappin et al. 1991; Chen et al. 2013). We propose here to test numerically the possibility that expansion is at the origin of some of the still not understood spectral properties, and focus on the scaling of the Elsasser spectra $E_\pm$, especially with strong Alfvénicity. We use 3D MHD simulations, with moderate ratio $B_0/b_{rms}$, with and without expansion. We find that with zero expansion, small-scale pinning of the dominant and subdominant spectra lead to (unobserved) different indices for the two Elsasser spectra, while with expansion, one finds nearly equal spectral exponents, as observed, and a slow spectral steepening with distance, thus leading naturally to the observed variability of spectral indices.

Keywords: Solar Wind, MHD, Turbulence, Alfvénicity, expansion

## 1 Introduction

Turbulence in the solar wind above sub-ion scales shows large variations of spectral properties with wind bulk speed and Alfvénicity at a given distance (Chen et al. 2013), and as well with heliocentric distance (Chen et al. 2020; Grappin et al. 1991). Attempts to interpret large-scale turbulence in terms of known MHD turbulence theories includes weak isotropic cascade ((Iroshnikov 1964; Kraichnan 1965), later IK), strong Kolmogorov cascade (K41), or more recently small-scale Alfvénic cascade (Boldyrev 2005). It appears difficult to reconcile the variety of observed indices with the precise predictions of the above mentioned theories: -3/2 for IK and small-scale Alfvénic cascade, -5/3 for K41.

However, the above mentioned theories don't take into account the expansion of the plasma due to the mean radial flow. We want here to test whether we recover or not the above mentioned properties when solving the 3D MHD equations including expansion (Grappin et al. 1993; Dong et al. 2014), and compare the result both with standard 3D MHD simulations and with the above mentioned solar wind spectral properties. We hope this will help to prove that expansion cannot be neglected in describing the turbulent cascade in the solar wind.

The expansion rate is measured by the expansion parameter $\epsilon$ which is the ratio of the initial nonlinear time $t_{NL} = 1/(k_0 u)$ of large eddies over the expansion time $t_e = R_0/U_0$ where $R_0$ is the initial heliospheric distance (here 0.2 AU) and $U_0$ the (assumed constant) average bulk solar wind speed.

In both the non-expanding and expanding cases, spectral evolution is followed during 10 nonlinear times. In the expanding case, during this time, the transverse plasma sizes will increase by a factor 5, corresponding to the heliospheric distance $R$ varying from 0.2 to 1 AU.

## 2 Definitions, parameters and Initial conditions

We first define the two Elsasser variables $z_\pm$:

$$z_\pm = u \mp sign(B_0)\delta B/\rho^{1/2} \tag{2.1}$$

[1] Laboratoire de Physique des Plasmas (LPP), CNRS, Observatoire de Paris, Sorbonne Université, Université Paris Saclay, Ecole Polytechnique, Institut Polytechnique de Paris, 91120 Palaiseau, France

[2] Università di Firenze, Dipartimento di Fisica e Astronomia, Firenze, Italy; INAF, OAA, Firenze, Italy

[3] Technische Universität Berlin, ER 3-2, Hardenbergstr. 36a, D-10623 Berlin, Germany; Max-Planck/Princeton Center for Plasma Physics

where $\delta B = B - B_0$ denotes the fluctuating magnetic field. The $z_+$ and $z_-$ denote respectively the amplitude of the outward and inward propagating Alfvén waves. The energies of the two Elsasser fields are $E_\pm = (1/2)z_\pm^2$. The Alfvénicity or normalized cross helicity is measured by

$$\sigma_c = (E_+ - E_-)/(E_+ + E_-) \tag{2.2}$$

We consider the following initial conditions for the homogeneous runs: magnetic and velocity fluctuation $b_{rms} = u_{rms} = 1$, a mean magnetic field $B_0$ between 1 and 5 times $b_{rms}$. The domain is elongated along the mean field with aspect ratio equal to $B^0/b_{rms}$ (fig.1a shows a case where $B_0 = 2$). The initial turbulent Mach number is $\delta u_{rms}/c_s$= 0.12, where $c_s$ is the sound speed.

In the expanding case (see Montagud-Camps et al. (2018)), the initial domain is elongated along the radial with an aspect ratio equal to 5, so that at the end of the computation the aspect ratio is unity, thus allowing more efficient nonlinear couplings at that time (fig.1b). The initial mean magnetic field has an small angle with the radial direction: $\vec{B_0}(t = 0) = B_0[1, 0.2, 0]$, such that at the end of the run it makes a $45^0$ angle with the radial. In most runs, we set $B_0$=2, but similar results are obtained with $B_0 = 1$ or 3.

Time $t$ is normalized by the initial nonlinear time, the relation between distance and time is:

$$R = R^0(1 + \epsilon t) \tag{2.3}$$

where $\epsilon = \frac{U^0/R^0}{k^0 u_{rms}} = 0.4$ is the ratio between the non-linear time and the linear expansion time.

Initial kinetic and magnetic fluctuations autocorrelation isocontours follow ellipsoids with the same aspect ratio as that of the simulation domain. The reduced 1D initial spectra $E_+(k)$ and $E_-(k)$ have the same initial spectral index, with the excitation being concentrated on first 32 modes in the expanding case, and the first 8 modes in the homogeneous case. Note that in the zero expansion case, we will consider spectra depending on $k_\perp$, i.e. the average of $E(k_y)$ and $E(k_z)$ spectra, while in the case with expansion we will consider spectra depending on $k_x$, corresponding to the radial component of the wavevector.

## 3 Results

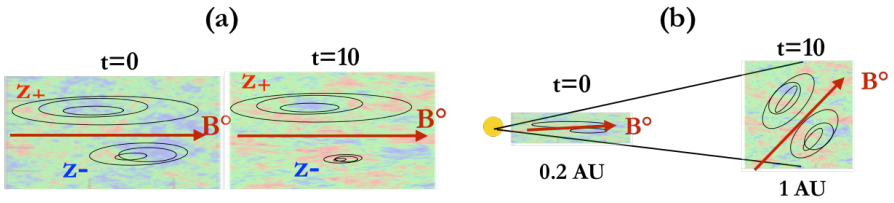


**Fig. 1.** Sketch of the evolution of the plasma volume: (a) Standard simulation; (b) simulation with expansion, Ox denoting the direction parallel to the radial; the domain expands in directions Oy and Oz as time/distance increase.

Fig. 2 shows $E_+(k)$ and $E_-(k)$ spectra, and the geometric mean $\sqrt{E_+E_-}$ at t=10, for five runs, with two values of the initial spectral index $m_0$, -5/3 and -1, and several values of $\sigma_c^0$. All runs show "pinning" of the $E_\pm$ spectra at dissipative scales, that is, spectra join there, i.e., cross helicity is zero at those scales. Cross helicity nevertheless remains at large scales. In the homogeneous case (top row), this leads to different spectral scalings for $E_+$ and $E_-$: the dominant $E_+$ spectrum is steeper than the $E_-$ spectrum, i.e., $|m_+| > |m_-|$. However, this is not so in the expanding case (bottom row): $E_+$ and $E_-$ spectra indeed separate, but the growth of cross helicity is limited by a secondary large-scale pinning effect, due clearly to expansion. In the following we choose to compute $E_\pm$ spectral indices ($m_\pm$) in the range $4 \leq k \leq 10$ (and we will call this range the inertial range) due to the reasonable constancy of indices in this range.

We first consider in fig. 3 some examples of the time evolution of $m_+$, the dominant spectrum index, varying again $m^0$ and $\sigma_c^0$, with the homogeneous runs in left panels (a), and runs with expansion right (b). We find (first panel) that the final scaling is quasi-independent of the initial scaling in non-expanding runs, which is expected, while on the contrary, in the expanding case (last two panels right), *the final scaling depends strongly on its initial value.*

Fig. 4 shows the evolution of the two $E_\pm$ spectral indices $m_\pm$ in different cases. The three left panels show runs without expansion with growing initial cross helicity from left to right, with two runs per panel, $m_0 = -1.2$

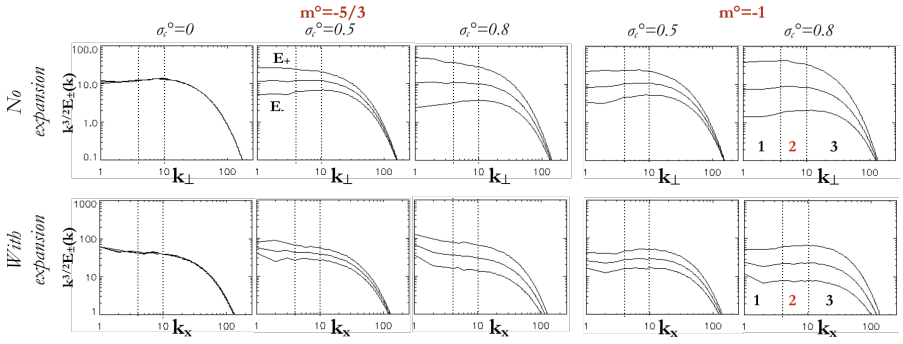


**Fig. 2.** Final (t=10) spectra: $E_+$, $E_-$ and geometric mean $\sqrt{E_+(k)E_-(k)}$, with inertial range indicated by dotted lines (k=4 and k=10). Top raw: zero expansion runs; bottom raw: runs with expansion. Spectra are compensated by $k^{-3/2}$.

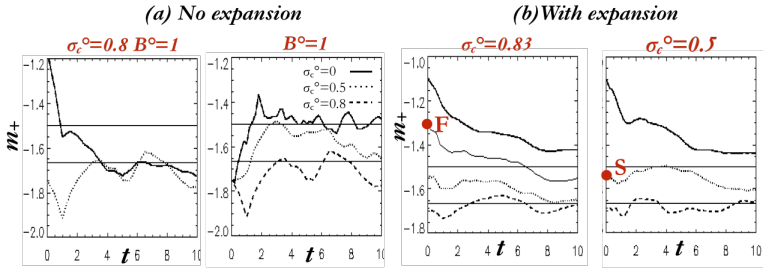


**Fig. 3.** Time evolution of the spectral index of the dominant energy ($E_+(k)$) illustrating the difference between the evolution (a) without and (b) with expansion, varying the initial index $m_+^0$ and cross helicity $\sigma_c^0$. Straight lines mark $m_+ = -1.5$ and -5/3.

(solid line) and $\simeq -5/3$ (dotted). Right panels show runs with expansion, all with large $\sigma_c^0$ (0.83) and different starting indices (an arrow is added to indicate the direction of motion). One sees for the non-expanding runs that the $m_-, m_+$ trajectories starting from $m_0 = -1.2$ and from $m_0 = -5/3$ join together close to the diagonal $m_+ + m_- = -3$, with the final attractor moving with growing $\sigma_c^0$ along the diagonal away from the central point $m_\pm = -3/2$ when $\sigma_c^0$ grows. This is the prediction of the weak isotropic turbulent regime (Grappin et al. (1983)). On the contrary, the four right panels (b) illustrate the formation of quasi-equal indices $m_\pm$ in the expanding case, with, again, the final index depending strongly on its initial value, confirming our earlier conclusion from fig. 3.

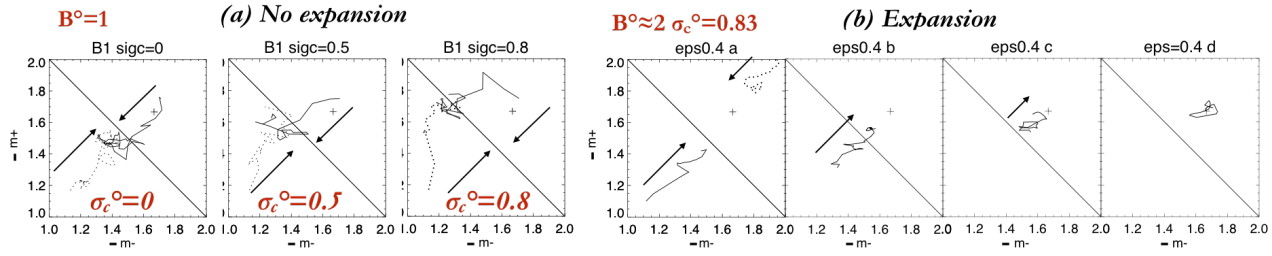


**Fig. 4.** Hodograms showing the evolution of the two spectral indices $m_\pm$ vs time, again illustrating the difference between (a) the zero expansion and (b) runs with expansion. Arrows indicate the direction of evolution. The cross represents $m_\pm = -5/3$ and the diagonal the line $m_+ + m_- = -3$.

Fig. 5 compares the $E_\pm$ spectra observed during the first four months of the Helios 2 mission (top row) with those obtained from simulations with expansion (bottom row). The bottom panels show spectra averaged within the following subsets, from left to right: *slow* streams close to the Sun and then far from Sun, *fast* streams close to the Sun and far from Sun. Helios data thus show the two properties remarked previously in our

simulations with expansion: (i) the two $E_+$ and $E_-$ spectra have comparable spectral indices; (ii) the "final" (close to Earth) scalings depend on the "initial" (close to Sun) scalings, considering the two subsets made of the fast (or highly Alfvénic) streams and slow (or mildly Alfvénic) streams. In our simulations, the corresponding test runs are denoted respectively run F and run S (see fig. 3).

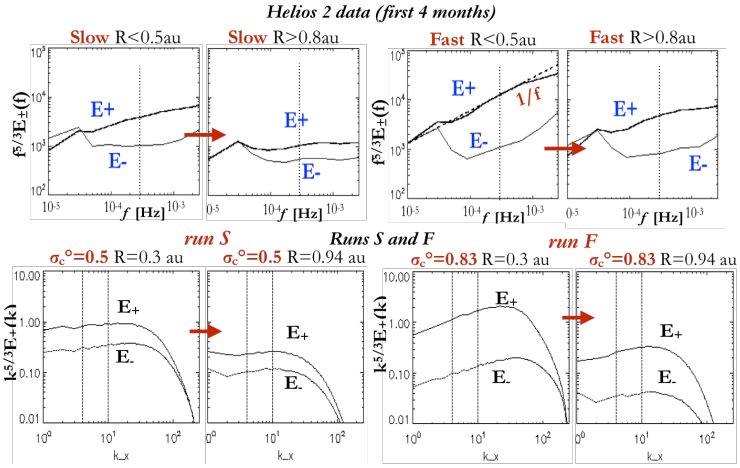


**Fig. 5.** Comparing $E_\pm(k)$ spectra (compensated by $k^{-5/3}$), respectively (a) in Helios data (top raw) and (b) in simulations with expansion (bottom). From left to right, Helios data show spectra averaged successively in slow streams close and far from the Sun, then in fast streams. Simulation data show spectra with low cross helicity close and far from the Sun, then the same with high cross helicity (see curves marked with S and F in fig. 3b).

## 4 Conclusions

We have considered here simulations of Alfvénic turbulence, with and without expansion. Our simulations show that 3D MHD simulations with expansion of the plasma volume (EBM) are able to reasonably reproduce the evolution of $E_\pm$ spectra in the inner heliosphere, as (i) similar indices for the two spectra, (ii) spectral indices varying slowly with distance, (iii) spectra becoming steeper with distance.

On the contrary, zero expansion simulations with cross helicity are dominated by the spectral pinning at dissipative scales, which leads to different spectral indices for the two $E_+$ and $E_-$ spectra, similar to that found in IK weak isotropic turbulence as generalized to Alfvénic turbulence by Grappin et al. (1983).

The interpretation of this quasi-isotropic behavior in a regime with non zero mean field, thus basically anisotropic, requires further analysis. This is true as well of the slow evolution observed here in the expanding case which is reminiscent of the freezing of shock waves found analytically with expansion (Grappin et al. 1993).

We thank Victor Montagud-Camps for useful remarks when reading the manuscript. This work was granted access to the HPC resources of IDRIS under the allocation 2020-A0090407683 made by GENCI.

## References

Boldyrev, S. 2005, The Astrophysical Journal, 626, L37
Chen, C., Bale, S., Bonnell, J. W., et al. 2020, The Astrophysical Journal Supplement Series, 246, 0
Chen, C., Bale, S., Salem, C. S., & Maruca, B. A. 2013, The Astrophysical Journal, 770, 125
Dong, Y., Verdini, A., & Grappin, R. 2014, The Astrophysical Journal, 793, 118
Grappin, R., Léorat, J., & Pouquet, A. G. 1983, ASTRONOMY AND ASTROPHYSICS, 126, 51
Grappin, R., Velli, M., & Mangeney, A. 1991, Annales Geophysicae, 9, 416
Grappin, R., Velli, M., & Mangeney, A. 1993, Physical Review Letters, 70, 2190
Iroshnikov, P. S. 1964, Soviet Astronomy, 7, 566
Kraichnan, R. 1965, Physics of Fluids, 8, 1385
Montagud-Camps, V., Grappin, R., & Verdini, A. 2018, The Astrophysical Journal, 853, 153